IOP Conf. Series: Materials Science and Engineering **818** (2020) 012019 doi:10.1088/1757-899X/818/1/012019

Ce and U speciation in wasteforms for thermal treatment of plutonium bearing wastes, probed by L_3 edge XANES

D J Bailey,[1] M C Stennett,[1] S K Sun,[1] L J Gardner,[1] S A Walling,[1] C L Corkhill,[1] B Ravel,[2] and N C Hyatt.[1]*

[1]Department of Materials Science & Engineering, The University of Sheffield, Mappin Street, Sheffield, S1 3JD.
[2]National Institute of Standards and Technology, Gaithersburg, Maryland 20899, USA.

*n.c.hyatt@sheffield.ac.uk

Abstract. X-ray absorption spectroscopy was applied to understand the speciation of elements relevant to the immobilisation and disposal of radioactive plutonium bearing wastes, utilizing Ce as a Pu surrogate. Ce L_3 XANES (X-ray Absorption Near Edge Structure) characterisation of a crystallised glass material produced by cold crucible plasma vitrification, at demonstration scale, evidenced incorporation as Ce^{3+} within the glass phase, providing an important validation of laboratory scale studies. U and Ce L_3 XANES investigation of brannerite ceramics, $U_{0.9}Ce_{0.1}Ti_2O_6$, synthesized under oxidizing, neutral and reducing conditions, established the charge compensation mechanism as incorporation of Ce^{3+} through formation of U^{5+} and/or U^{6+} In each of these examples, X-ray Absorption Spectroscopy has provided a pivotal understanding of element speciation in relation to the mechanism of incorporation within the host wasteform intended for geological disposal.

1. Introduction

The UK is engaged in a programme of decommissioning, clean up and disposal of legacy facilities and materials from over five decades of nuclear fuel cycle activities. This programme will extend over more than 120 years and cost in excess of £115 billion [1]. The UK radioactive waste inventory comprises a spectrum of plutonium bearing wastes, which include plutonium residues and plutonium contaminated materials (PCM), generated by reprocessing of nuclear fuel [2-8]. The inventory of plutonium and Mixed Oxide (MOX) fuel residues is of the order of 0.5 t and includes material from which plutonium recovery is considered uneconomic [2], including PuO_2 which is heavily contaminated by chlorine as a result of long term storage in PVC packaging which has degraded. The inventory of untreated PCM waste comprises in excess of 20,000 m^3 on the Sellafield site alone [5].

A tool box of thermal treatment technologies is under development for conditioning of plutonium / MOX residues and PCM wastes, as well as other complex higher activity wastes, which are incompatible with cement encapsulation [2-13]. Primary drivers for the application of thermal treatment processes include the reduced volume, improved passive safety, and superior long term stability of the waste form products [3]. These benefits arise from destruction of the organic waste fraction, oxidation of the metal waste component, and evaporation of entrained water, in tandem with the immobilisation of radioactive and chemotoxic elements within a durable ceramic, glass, or glass-ceramic material.

Here, we demonstrate the crucial role of X-ray absorption spectroscopy in understanding plutonium surrogate and contaminant speciation in wasteforms designed for immobilisation of PCM wastes and plutonium / MOX residues by thermal treatment: a crystallised glass (or slag) waste form, produced by cold crucible plasma vitrification at the demonstration scale, to immobilise PCM wastes; and a ceramic waste form, produced by cold pressing and sintering at the laboratory scale, tailored to immobilise MOX fuel residues. In each case study, the critical role of speciation, determined by X-ray Absorption Spectroscopy, in controlling the incorporation mechanisms, is emphasised.

2. Experimental

2.1 Plasma vitrified wasteforms

A simulant PCM waste, using CeO_2 as a PuO_2 surrogate, was vitrified using a twin torch plasma system, at waste loadings of 31, 40 and 54 wt% PCM waste, with glass forming additives (CaO 29.2 %, Al_2O_3 27.7 % and SiO_2 43.1 % by weight). The slag melt was maintained at ca. 1500ºC in the cold crucible and quenched to form a glassy solid, as previously described [9]. Ce L_3 edge (5723.4 eV) XANES data from plasma vitrified products, and reference compounds, were acquired from polished solid specimens on Beamline 9A of the Photon Factory, Japan. The configuration utilised: Si (111) double crystal monochromator; harmonic rejection mirror; ion chambers (I_0), and 19 element Ge solid-state fluorescence detector [14]. Samples were prepared by diluting the material to be investigated in polyethylene glycol to yield a thickness of $\mu x = 1$. All XANES data were dead time corrected and processed in Athena using standard background subtraction and normalisation procedures [15].

2.2 Brannerite ceramic wasteforms

Reagents (UO_2, CeO_2, TiO_2) were combined in stoichiometric ratio with isopropanol to form a slurry and ball milled for 5 min at 30 Hz using a Fritsch Pulverisette 23. The dried slurry was calcined at 1300ºC for 12 h and sintered at 1320ºC for 12 h; heat treatments were performed under air, Ar or 5 % H_2 / N_2 atmosphere. U and Ce L_3 edge XANES data from brannerite ceramics and reference compounds were acquired in transmission and fluorescence mode, respectively, on the now decommissioned beamline X23A2 of the National Synchrotron Light Source, USA [16]. The configuration utilised: Si (311) double crystal monochromator; Rh harmonic rejection mirror; ion chambers (I_0, I_t, I_{ref}). U L_3 edge XANES (17166.3 eV) were acquired in transmission mode whereas Ce L_3 edge XANES (5723.4 eV) were acquired using a four element Vortex Si-drift detector in fluorescence mode with the aid of a harmonic rejection mirror. Additional U L_3 edge XANES data were acquired, using the same procedure, on the 6-BMM, National Synchrotron Light Source II, using a double crystal Si (111) monochromator. Reference compounds were synthetic $CePO_4$, CeO_2, UTi_2O_6, $U_{0.5}Y_{0.5}Ti_2O_6$, and $CaUO_4$. Samples were prepared for XANES analysis by diluting the material to be investigated in polyethylene glycol to yield a thickness of $\mu x = 1$. All XANES data were dead time corrected and processed in Athena using standard background subtraction and normalisation procedures [15].

2.3 General characterization methods

Scanning Electron Microscopy (SEM) coupled with Energy Dispersive X-ray (EDX) analysis was performed on polished and carbon coated specimens, using a Hitachi TM3030 SEM with a 15 kV accelerating voltage and a working distance of 8 mm. Compositional analysis was conducted with a Bruker Quantax EDX system. Samples were ground and sieved for powder X-ray diffraction (PXRD) using a Bruker D2 PHASER diffractometer with Ni filtered Cu Kα radiation (1.5418 Å); data were acquired between $10° \leq 2\theta \leq 70°$, with a step size of 0.02°, using a Lynxeye position sensitive detector.

3. Results and discussion

3.1 Plasma vitrified wasteforms

Cold crucible plasma arc vitrification is a candidate technology for thermal treatment of plutonium contaminated material (PCM) wastes, to produce a partially crystallised glass (or slag) waste form [9]. In this study, the speciation of Ce, as a Pu analogue, was investigated in the slag products of cold crucible

plasma arc vitrification, produced at demonstration scale, with 31, 40 and 54 wt% simulant PCM waste, and glass forming additives (CaO 29.2 %, Al_2O_3 27.7 % and SiO_2 43.1 % by weight). Details of the waste simulant composition and a comprehensive study of the slag microstructure, phase assemblage and composition were published previously [9].

Figure 1 shows, as an example, the microstructure of the 54 wt% PCM slag, which comprises two amorphous components with light and mid grey contrast; EDX showed the phase of lighter contrast (A) was depleted in Al_2O_3 and enriched in Fe_2O_3, compared to the phase of darker contrast (B). Additional crystalline phases of mullite, anorthite, alumina, and spinel were identified by PXRD, evident in the microstructure as angular dark grey features (e.g. C). EDX demonstrated Ce to partition exclusively to the amorphous phases, with no preference for either amorphous component within the margin of precision [9]. The composition and microstructure of all slag materials were similar, though with increasing amorphous fraction with decreasing waste loading, as assessed from SEM/EDX and PXRD.

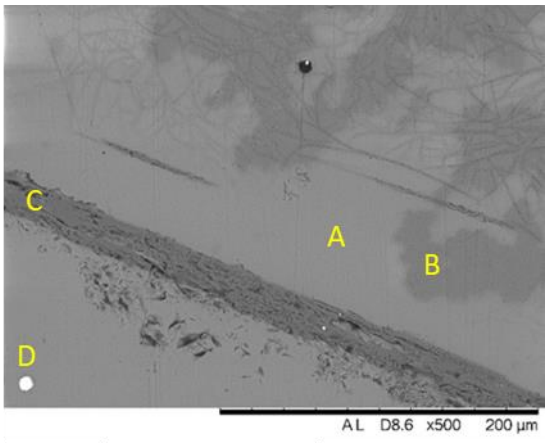

Figure 1. Microstructure (back scattered electron image) of plasma vitrified simulant PCM waste (54% waste loading by weight), comprising two amorphous components (A and B); crystalline mullite, anorthite, alumina, and spinel phases (C), and a ferrous alloy (D)**.**

Ce L_3 edge XANES data, Figure 2, were acquired to determine the Ce speciation in the amorphous phase. The low Ce concentration (ca. 0.6(2) mol % CeO_2 determined by EDX) required data acquisition in fluorescence mode, which was limited to the XANES region due to edge overlap by trace Cr_2O_3 in the material. The Ce L_3 XANES features and edge shift of all slag compositions closely resemble those of Ce^{3+} in $CePO_4$ monazite, characterised by a single intense feature attributed to the transition from an initial $2p^64f^15d^0$ state to a $2p^54f^15d^1$ final state [17-19]. In contrast, the Ce L_3 edge XANES of Ce^{4+} in CeO_2 is characterised by a white line comprising two features of lower relative intensity due to transition from an initial $2p^64f^05d^0$ state to: (A) the $2p^54f^05d^1$ final state; and (B) the $2p^54f^15d^1L^1$ final state (where L^n denotes a ligand hole); feature C is associated with transition to a $2p^54f^25d^1L^2$ final state, whereas D is assigned to quadrupole transition [17-19]. The XANES spectra shown in Figure 5 permit straightforward fingerprinting of the Ce oxidation state. From comparison of the spectra it is apparent that the XANES data of slag fraction closely resemble that of $CePO_4$, demonstrating that Ce^{3+} is the dominant species, no significant Ce^{4+} contribution was determined by linear combination fitting of the XANES data of $CePO_4$ and CeO_2 reference compounds.

Previous Ce L_3 edge XANES characterisation of slag wasteforms produced by laboratory scale crucible melts utilising a wider spectrum of simulant PCM wastes, and a closely related glass composition, also demonstrated Ce partitioning to the glass phase exclusively as reduced Ce^{3+} [5]. The solubility of Ce_2O_3 and Pu_2O_3 in (boro)silicate glasses has been shown to be broadly similar, with an upper limit of ca. 2 mol% at 1450 °C [20]. Thus, our speciation data provide confidence of Pu incorporation within the glass component of the slag phase in the proposed plasma treatment process, since the incorporation rate is expected to be well below the anticipated solubility limit, given the evidently reducing nature of the melt.

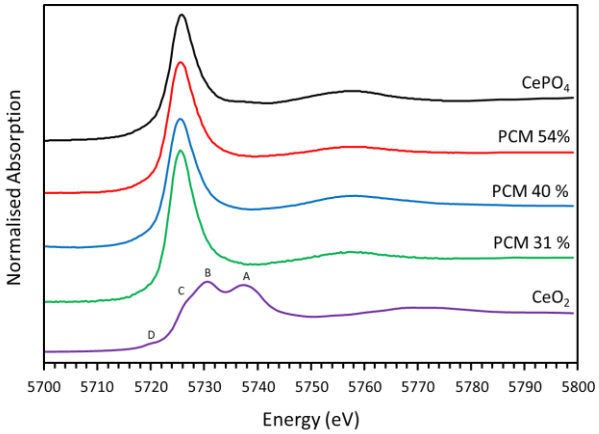

Figure 2. Ce L_3 edge XANES data acquired from plasma vitrified simulant PCM waste, with 31 wt%, 40 wt% and 54 wt% waste loading by weight, compared with CeO_2 and $CePO_4$ reference compounds, see text for detail.

3.2 Brannerite ceramic wasteforms

Brannerite, prototypically UTi_2O_6, is a potential ceramic host for residues arising from MOX (Mixed Oxide, $(Pu,U)O_2$) fuel fabrication [8, 21]. The crystal structure of brannerite comprises layers of anatase-like edge sharing TiO_6 octahedra which are linked by UO_6 octahedra that also share edges [8, 21]. In this exploratory study, we investigated the synthesis of brannerites formulated $U_{0.9}Ce_{0.1}Ti_2O_6$, under air, argon and 5 % H_2 / N_2 atmosphere, with Ce as a Pu surrogate at realistic concentration. Representative microstructures of ceramics sintered at 1320 ^oC for 12 h are shown in Figure 3: synthesis under air (Fig. 3a) afforded U_3O_8 as the major phase (A) with minor brannerite (B) and rutile (R); whereas, synthesis under argon and 5 % H_2 / N_2 (Fig 3b and 3c, respectively) produced brannerite as the major phase (B), with minor rutile (R) and trace UO_2 (C). Ce was determined to partition exclusively to the brannerite phase by EDX spot analysis and mapping, Figure 3. The phase assemblages were confirmed by PXRD.

Ti K, Ce L_3 and U L_3 XANES were exploited to understand the charge compensation mechanisms and phase assemblages in $U_{0.9}Ce_{0.1}Ti_2O_6$ brannerite ceramics. Ce L_3 edge XANES of the brannerite ceramics, Figure 4, revealed reduction of Ce^{4+} to Ce^{3+} under all processing conditions, by comparison with data from $CePO_4$ and CeO_2 (reference compounds for Ce^{3+} and Ce^{4+}, respectively). The U L_3 XANES of brannerites synthesised in 5 % H_2 / N_2 and argon showed an edge shift comparable to that of the UTi_2O_6 reference, Figure 5, whereas that of the brannerite sintered under air showed an edge shift between $Y_{0.5}U_{0.5}Ti_2O_6$ and $CaUO_4$. Linear regression of oxidation state versus edge shift for the reference compounds enabled the average U oxidation state of the brannerite compounds to be determined as 5.4+ for the air processed material and 4.1+ and 4.0+ for the samples produced under argon and 5 % H_2 / N_2, respectively (± 0.1). Ti K edge XANES data (not shown) revealed the Ti oxidation state in the brannerites to be 4.0+, within precision, irrespective of the processing atmosphere.

Near single phase $U_{0.9}Ce_{0.1}Ti_2O_6$ brannerite could evidently only be synthesised under argon or 5 % H_2 / N_2 atmosphere. The observed reduction of Ce^{4+} to Ce^{3+} implies charge compensation by marginal oxidation of U^{4+}, which was within the uncertainty of the U oxidation state determined by U L_3 XANES. Under air atmosphere the average U oxidation state was 5.4+, consistent with the coexistence of U_3O_8, and the Ce rich brannerite stoichiometry determined by EDX thus implies charge compensation by U^{5+} and/or U^{6+}.

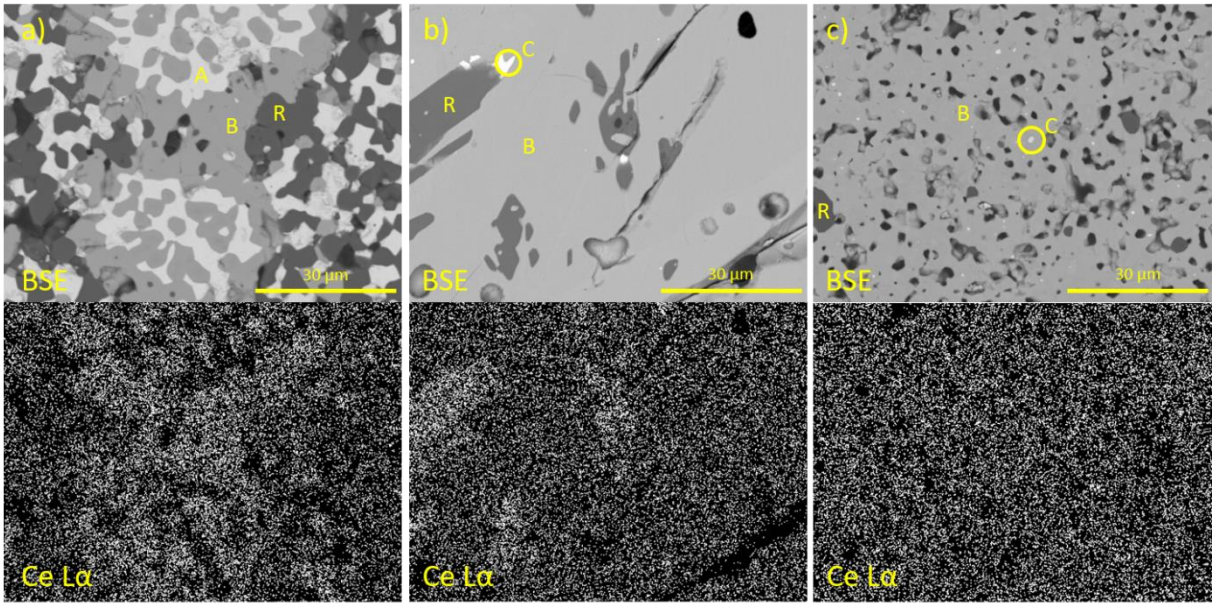

Figure 3. Microstructures (back scattered electron images) of brannerite ceramics with formula $U_{0.9}Ce_{0.1}Ti_2O_6$ synthesised under a) air, b) argon and c) 5 % H_2 / N_2 atmosphere; A = U_3O_8, B = $(U,Ce)Ti_2O_6$, R = TiO_2, Rutile; C = UO_2. Note overlap of Ti Ka and Ce La emission lines gives rise to apparent Ce incorporation in rutile phase.

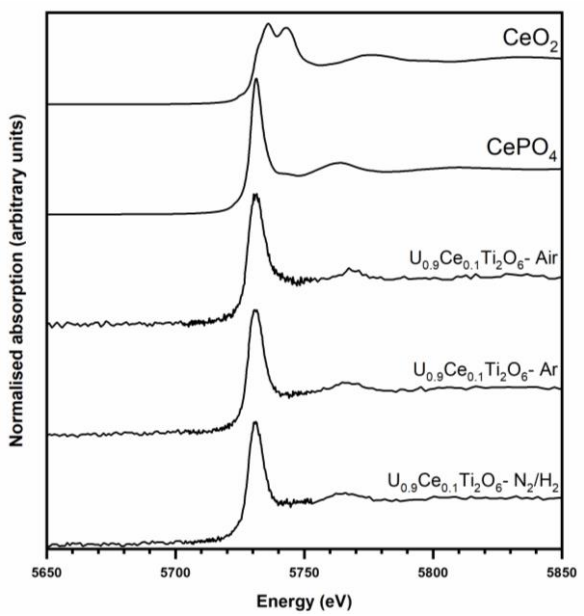

Figure 4. Ce L_3 XANES of brannerite ceramics sintered under air, argon, or 5% H_2 / N_2 atmosphere, plus reference compounds $CePO_4$ and CeO_2.

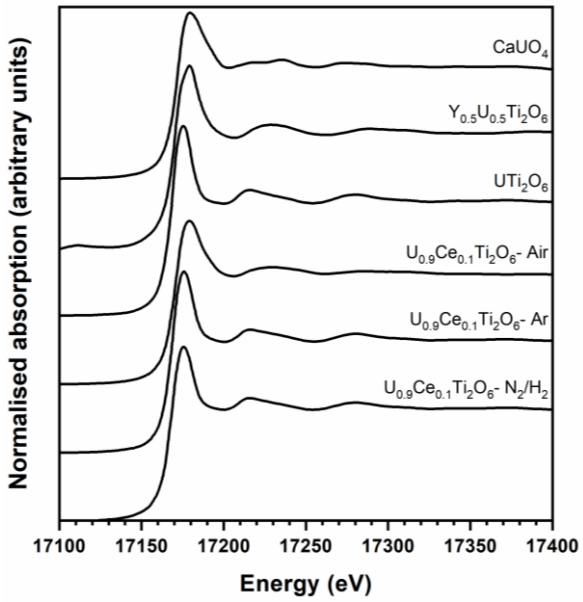

Figure 5. U L_3 XANES of brannerite ceramics sintered under air, argon, or 5 % H_2 / N_2 atmosphere, plus reference compounds UTi_2O_6, $U_{0.5}Y_{0.5}Ti_2O_6$, and $CaUO_4$.

4. Conclusions

The Ce L_3 edge XANES data of slag wasteforms produced by cold crucible plasma vitrification, provide a useful and essential verification of Ce partitioning and reduction in a demonstration scale cold crucible processing, which was not sensitive to waste loading. The common Ce^{3+} speciation achieved in demonstration and laboratory scale slag wasteforms produced from thermal treatment of simulant PCM waste, results in exclusive partitioning to the glass phase under the reducing melt conditions. This observation provides important confidence that laboratory scale crucible melts provide a useful guide to surrogate partitioning behaviour in demonstration and full scale processing, in early stage research and development.

We have shown that near single phase brannerite ceramics may be fabricated by a cold-press and sinter process under neutral to reducing atmosphere, as effective candidate waste forms for MOX residue immobilisation, with waste loading of up to ca. 63 wt%. The ability of the brannerite structure to self charge compensate for potential reduction of Pu^{4+} to Pu^{3+} (as demonstrated by the Ce analogue), through oxidation of U^{4+} to U^{5+} and/or U^{6+} is an attractive feature and would mitigate against variations in U / Pu feed composition within solid solution limits (as could be expected with residues of variable Pu content). Overall, this is a promising approach since the cold-press and sinter processing technology is already implemented for MOX fuel manufacture and a fuel processing plant could conceptually be repurposed for an immobilisation mission at the end of fuel production operations.

5. References

[1] Nuclear Decommissioning Authority, 2016. Strategy, Effective from April 2016.
[2] Scales, C R, Maddrell, E, Gawthorpe, N, Begg, B D, Moricca, S, Day, R A and Stewart M W 2006 *Waste management '06, WM'06*, Feb 26- Mar. 2, 2006, at Tucson AZ, USA, 6232.
[3] Thornber, S M, Heath P G, Maddrell E R, Stennett M C and Hyatt N C 2016 *MRS Advances* **1** 4269.
[4] Thornber S M, Heath P G, Da Costa G P, Stennett M C and Hyatt N C 2017 *J. Nucl. Mater.* **485** 253.
[5] Hyatt N C, Schwarz R R, Bingham P A, Stennett M C, Corkhill C L, Heath P G, Hand R J, James M, Pearson A and Morgan S 2017 *J. Nucl. Mater.* **444** 186.
[6] Thornber S M, Stennett M C, Vance E R, Chavara D T, Watson I, Jovanovic M, Davis J, Gregg D and Hyatt N C 2018 *MRS Advances* **3** 1065**.**

[7] Hyatt N C 2017 *Energy Policy* **101** 303.
[8] Bailey D J, Stennett M C, Ravel B, Grolimund D and Hyatt N C 2018 *RSC Advances* **8** 2092.
[9] Hyatt N C, Morgan S, Stennett M C, Scales C R and Deegan D 2007 *MRS Symp. P.* **985** 393.
[10] Bingham P A, Hand R J and Hyatt N C 2012 *Glass Technol. Part A* **53** 83.
[11] Bingham P A, Hyatt N C, Hand R J and Forder S D 2013 *Glass Technol. Part A* **54** 1.
[12] Hyatt N C and James M 2013 *Nucl. Eng. Inter.* **58** 10.
[13] Heath P G, Stewart M W A, Moricca S and Hyatt N C 2018 *J. Nucl. Mater.* **499** 233.
[14] Nomura M and Koyama A 1999 *J. Synchrotron Rad.* **6** 182.
[15] Ravel B and Newville M 2005 *J. Synchrotron Rad.* **12** 537.
[16] Long G G, Allen A J, Black D R, Burdette H E, Fischer D A, Spal R D and Woicik, J C 2001 *J. Res. Nat. Inst. Stand. Tech.* **106** 1141.
[17] Bianconi A, Marcelli A, Dexpert H, Karnatak R, Kotani A, Jo T and Petiau J 1987 *Phys. Rev. B* **35** 806.
[18] Soldatov A V, Ivanchenko T S, Della Longa S, Kotani A, Iwamoto Y and Bianconi A 1994 *Phys. Rev. B* **50** 5074.
[19] Stennett M C, Freeman C L, Gandy A S and Hyatt, N C 2012 *J. Solid State Chem.* **192** 172.
[20] Lopez C, Deschanels X, Bart J M, Boubals J M, Den Auwer C and Simoni E 2003 *J. Nucl. Mater.* **312** 76.
[21] Bailey D J, Stennnett M C and Hyatt N C 2016 *Procedia Chem.* **21** 371.

Acknowledgment
This research was sponsored in part by EPSRC under grant references EP/L015390/1, EP/R512175/1, EP/N017374/1, EP/P013600/1, and EP/S01019X/1. This project received funding from the Euratom Research and Training Programme 2014-18, (Grant Agreement No. 755480 and the 7th Framework programme (Grant agreement No. 323300). This research accessed beamline BMM of the National Synchrotron Light Source II, a U.S. Department of Energy (DOE) Office of Science User Facility Operated for the DOE office of Science by Brookhaven National Laboratory under Contract No. DE-SC0012704. This research utilised the HADES / MIDAS Facility, established with financial support from the UK Department for Business, Energy and Industrial Strategy and EPSRC under grant reference EP/T011424/1.